J. Astrophys. Astr. (1987) **8,** 263–270

Study of Electron Energy and Angular Distributions and Calculations of X-ray, EUV Line Flux and Rise Times

Ranjna Bakaya, Sunil Peshin, R. R. Rausaria & P. N. Khosa
Department of Physics, Regional Engineering College, Hazratbal, Srinagar, Kashmir 190006

Received 1986 December 27; accepted 1987 June 7

Abstract. Evolution of energy and angular distributions of electrons has been studied by combining small-angle analytical treatment with large-angle Monte Carlo calculations as a function of column density for initially monoenergetic and monodirectional electrons. The incident electron energies considered are 20, 30 and 60 keV at 0°, 30° and 60° angles of incidence. Using these distributions, time evolution of extreme ultraviolet (EUV) spectrum has been studied. The slopes of the curves calculated compare well with the experimentally observed curve.

Key words: Sun, X-ray bursts—Sun, EUV flares

1. Introduction

One of the most interesting properties of solar hard X-ray bursts, is their synchronism with the impulsive extreme ultraviolet (EUV) flare emissions observed by means of their effect on the ionosphere which manifests itself in the form of sudden frequency deviations (SFD's) in radio transmission (Kane 1974; Donnelly 1970; Kane & Donnelly 1971). The hard X-ray bursts ($\gtrsim$ 10 ke V) are generally attributed to collisional bremsstrahlung of nonthermal electrons in the flare plasma while the EUV emissions are thought to arise thermally by free-bound and line transitions in the broad wavelength range (10–1030 A) to which the ionosphere is sensitive. Thus the study of these synchronous emissions provides valuable insight into the connection between the nonthermal and thermal aspects of the flare.

Kane & Donnelly (1971) studied the relationship between impulsive solar EUV bursts observed by means of SFD's and hard X-ray bursts (energies $\geqslant$10 keV) recorded mainly by single-channel ionization chambers aboard OGO 1 and OGG 3, and in a few cases by the OGO 5 multichannel measurements.

Generally, the EUV bursts show very good time coincidence with the nonthermal hard X-ray and the impulsive microwave bursts (Fig. 1). If the hard component is not present in the X-ray enhancement, an EUV burst may still be observed, but such a burst is usually weaker and rises more slowly to the maximum than the EUV bursts associated with impulsive X-ray events. Therefore, as in the X-ray, region, the bursts appear to have two components—one of nonthermal and impulsive nature, and the other of quasi-thermal and gradual character (Castelli & Richards 1971; Wood & Noyes 1972; Donnelly *et al.* 1973). Since very little is known about the relatively weak

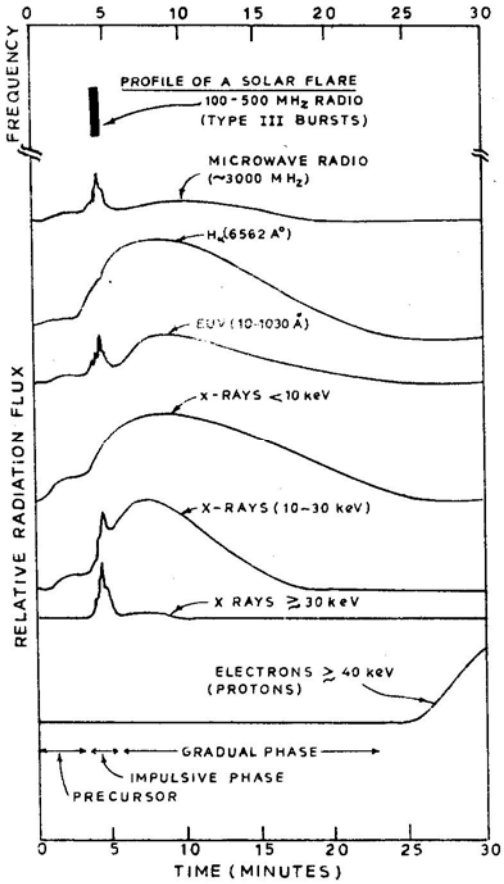

Figure 1. Schematic representation of the different phases of a solar flare as observed in the electromagnetic and particle radiation (after Kane 1974).

gradual EUV bursts that accompany the soft X-ray bursts and microwave post-burst increase, we shall confine our discussion only to the typical impulsive EUV enhancements.

The EUV emission appears in many Spectral lines ranging from those of neutral hydrogen and oxygen to highly ionized species such as Si XII and Fe XV and Fe XVI as well as in the recombination continua of neutral hydrogen and helium. In strong events, continuous emission other than radiative recombination continua also contributes to EUV burst. X-ray emissions from solar flares in the spectral range 1–10 keV is usually interpreted as being produced by a thermal plasma at several million degrees of temperature. Furthermore, line emission of these photon energies cannot be explained in terms of isothermal models of flares and instead multitemperature models have to be postulated (Meekins *et al.* 1970; Neupert 1971). For these reasons, it seems necessary to investigate the ionization and recombination processes which occur in ä plasma whose electrons follow a non-Maxwellian energy distribution. The EUV flux depends on the nature of electron energy distributions. The EUV generation due to power law spectrum has been studied by Landini, Monsignori Fossi & Pallavicini (1973) and

Haug (1979). However, in these studies the effect of multiple scattering on electron energy distributions has not been considered. The intent of the present paper is to study the EUV emission with the help of nonthermal distributions accounting for the dispersion in electron energy and angles resulting from multiple collisions.

2. Electron Energy and Angular Distributions

Usually, the energy spectrum of the nonthermal electrons is deduced from measured X-ray spectra. The electron energy spectrum above 10 keV is taken to be of a power law form. We have considered initially monoenergetic incident beams of electrons having energies 20, 30 and 60 keV characterized by a velocity vector $\hat{\mathbf{n}}$. The choice of monoenergetic beam is justified by the fact that the power law shape of distribution can be obtained by giving suitable weights to monoenergetic electrons. The components of $\hat{\mathbf{n}}$ in a co-ordinate system with z-axis are $\sin\alpha\cos\phi$, $\sin\alpha\sin\phi$ and $\cos\alpha$ where α is the angle of incidence with respect to vertical direction and becomes the pitch angle in the presence of a magnetic field. We consider the electrons directed towards the chromosphere, from the acceleration site situated in corona at 0°, 30° and 60° angles of incidence. Electron transport has been calculated as a function of column density/ height in the atmosphere.

We consider a fully ionized thermal plasma consisting of protons and electrons. It is assumed that the relativistic electron beam will be influenced only by Coulomb forces between the beam electrons and the thermal protons and electrons. Since for chromospheric and coronal plasma, the mean free path as determined by the minimum scattering-angle, is only a small fraction of a centimetre, it is not possible to treat all the small-angle deflections in a pure Monte Carlo procedure. The path of electrons is, therefore, divided into two parts: a condensed history of the small-angle scattering processes treated analytically, followed by Monte Carlo calculations of a single large-angle collision process. Details of the calculations are given in Haug, Elwert & Rausaria (1985) and Koul *et al.* (1985).

In the condensed history, the numerous collision processes with small energy losses are taken into account by mean energy loss rates. We have considered electrons starting at the location $S = 0$, which is taken as the acceleration site situated high up in the corona. In the case of horizontal stratification, S is the height in the atmosphere counted positive downwards (towards the chromosphere). The relation between S and path length is $S = l\cos\theta$ where θ is the angle between electron direction and gradient $\hat{\mathbf{n}}$. The random walk of each electron is followed towards the chromosphere until it has lost nearly its total energy ($E < E_{\min}$); $E_{\min}$ is ~ 5 per cent of the initial energy E_0. It is turned out that for all scale heights used the results depend only on column density $N(S) = \int_0^S n(S)\mathrm{d}S$, the number of protons/cm^2 or electrons/cm^2 within the column traversed. By this procedure we determine the electron energy and angular distributions at different heights (See Haug, Elwert & Rausaria 1985 for detail). A look at the distributions shows that electrons coming at 60° incidence are stopped at higher heights (lower column density) and electrons with 0° incidence are stopped at lower heights (higher column density) (Koul *et al.* 1985). However, the general trend of energy and angular distributions remains the same, becoming broader with the increase in the depth of penetration for all the incidence angles and energies of electrons (Koul *et al:* 1985; Haug, Elwert & Rausaria 1985). The number of backscattered electrons,

however, increases for higher incidence angles. Some examples of electron-energy distributions at different heights for given initial energy and incident angle are shown in Fig. 3. The number of particles followed is 10^4.

3. Calculations of Line Flux and its Comparison with Experimental Data

We have considered Si xiv and Fe xxv for the calculation of EUV flux. For such highly ionized atoms, it is sufficient to evaluate the strength of an emission line in a two-level approximation including the ground and the excited level, *i.e.,* neglecting cascades via energetically higher configurations. Following the reasoning on the lines of Haug (1979) in this work also, it is assumed that the ionization equilibrium of the coronal plasma is established predominantly by thermal processes and is not much influenced by direct ionization due to nonthermal electrons. The flux of line photons including the backscattering correction factor C_R is given by Haug (1979) as

$$F_{kl} = \frac{3\pi}{16\alpha^3}\frac{B_{lk}}{g_k}\frac{N_{iz}}{N_i}\frac{\varepsilon_i}{\sum_i \varepsilon_1 z_i}\frac{\gamma-1}{B(\gamma-1,\frac{1}{2})}\frac{k}{C_R}E_{kl}^{-(\gamma-1)}\langle\Omega_{kl}\rangle$$

$$= 1.11\times 10^6 \frac{B_{lk}}{g_k}\varepsilon_i\frac{N_{iz}}{N_i}\frac{\gamma-1}{B(\gamma-1,\frac{1}{2})}\frac{k}{C_R}E_{kl}^{-(\gamma-1)}\langle\Omega_{kl}\rangle$$

photons cm $^{-2}$ s^{-1} (1.1)

where the symbols have the same meaning as in Haug (1979). Haug (1979) has further shown that the same expression is valid for thick target geometry also.

Using Equation (1.1) and the electron energy distributions we have studied F_{kl} as function of column density. We have calculated the electron energy and angular distribution with a given initial energy and incidence angle. Initially the calculations have been done for monoenergetic electrons. Then we have extended the calculations to incorporate the power-law nature of the electron distribution. In this case also to start with we take a constant value of spectral index. However, as the electrons penetrate the deeper layers of the Sun, there is dispersion in energy of the electron as a result the spectral index changes. At each column we have computed the change in the spectral index and have used this value for calculation of line flux. To check the validity of our calculations, we have compared the line flux with OSO-5 observations. The results are given in Tables 1–3. From the tables one can see that the calculated values are close to observations showing that the contribution of nonthermal electrons for the production of X-ray and EUV line flux is significant.

4. Rise times

The rise of EUV emission is compared with the rise of hard X-ray emission for the various energy bands of the OGO 5 measurements for three flares in Fig. 2, where the fluxes were corrected by removing the pre-flare background. The rise of impulsive EUV emission was found to be usually similar to that of the 9.6–19.2 keV X-rays. In some flares, this close agreement extended to the 19.2-32 keV X-rays, while in other bursts,

Table 1. Line flux F_{kl} for Si xiv.

S. No.	γ	Column density	Electrons incident at 0°	30°	60°
I	3	0.16×10^{20}	1.84×10^{5}	1.79×10^{5}	2.25×10^{5}
		0.62×10^{20}	4.23×10^{5}	3.63×10^{5}	5.89×10^{5}
		0.89×10^{20}	5.42×10^{5}	6.74×10^{5}	9.12×10^{5}
II	4	0.16×10^{20}	1.18×10^{4}	1.12×10^{4}	1.46×10^{4}
		0.62×10^{20}	3.22×10^{4}	2.85×10^{4}	5.26×10^{4}
		0.89×10^{20}	4.76×10^{4}	5.95×10^{4}	9.76×10^{4}
III	5	0.16×10^{20}	6.30×10^{2}	6.90×10^{2}	8×10^{2}
		0.62×10^{20}	2.03×10^{3}	1.85×10^{3}	3.91×10^{3}
		0.89×10^{20}	3.45×10^{3}	4.37×10^{3}	8.7×10^{3}

Table 2. Line flux F_{kl} for Fe xxv.

S. No.	γ	Column density	Electrons incident at 0°	30°	60°
I	3	0.16×10^{20}	1.17×10^{3}	1.10×10^{3}	1.56×10^{3}
		0.62×10^{20}	2.69×10^{3}	2.31×10^{3}	3.75×10^{3}
		0.89×10^{20}	3.47×10^{3}	4.29×10^{3}	5.81×10^{3}
II	4	0.16×10^{20}	7.54×10^{1}	7.14×10^{1}	9.30×10^{1}
		0.62×10^{20}	2.06×10^{2}	1.81×10^{2}	3.88×10^{2}
		0.89×10^{20}	3.03×10^{2}	3.79×10^{2}	4.72×10^{2}
III	5	0.16×10^{20}	0.40×10^{1}	0.38×10^{1}	0.50×10^{1}
		0.62×10^{20}	1.3×10^{1}	1.18×10^{1}	2.49×10^{1}
		0.89×10^{20}	1.82×10^{1}	2.78×10^{1}	5.56×10^{1}

Table 3. Line flux F_{kl} for $\gamma = 4$.

S. No.	λ(Å)	Column density	Electrons incident at 0°	30°	60°
Fe xxv:					
I	1.850	0.62×10^{20}	3.25×10^{2}	3.42×10^{2}	1.17×10^{3}
		0.89×10^{20}	5.25×10^{2}	8.73×10^{2}	1.73×10^{3}
II	1.513	0.62×10^{20}	3.10×10^{2}	2.99×10^{2}	9.59×10^{2}
		0.89×10^{20}	4.80×10^{2}	7.75×10^{2}	1.48×10^{3}
Si xxv:					
I	2.01	0.76×10^{20}	1.38×10^{5}	3.32×10^{5}	5.36×10^{5}
		0.89×10^{20}	1.88×10^{5}	4.58×10^{5}	8.1×10^{5}

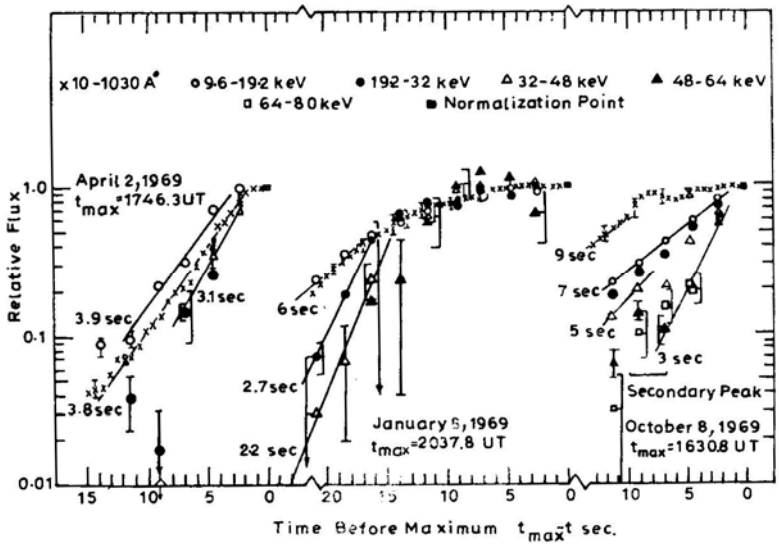

Figure 2. Impulsive solar EUV and hard X-ray bursts—rise time comparisons.

the rise of EUV emission was slower than that in hard X-rays for energy bands greater than 32 keV. These results are independent of the small uncertainity in the EUV rise resulting from uncertainities in the ionospheric electron loss rates involved in the analysis of each particular SFD.

The fact that the impulsive EUV emission rises and decays slower than the X-ray above 32 keV should not be interpreted to mean that these EUV emissions are like the slow flare emissions observed at soft X-ray and EUV wavelengths. The rise times for the impulsive bursts discussed above range from several seconds to several tens of seconds, while the time constants for the slow soft X-ray and EUV emission are typically several minutes for rise times and upto several tens of minutes for decay times.

5. Results and discussion

Using the electron distributions calculated in Section 2 we have studied the rise times of EUV bursts. A look at the observed time profiles of EUV shows that it is steeper in the beginning and becomes flatter afterwards. To explain this, we have taken electron energy distributions in a fixed energy interval with initial electron energies of 20, 30, 60 keV as function of height. By taking slopes of energy distributions we find that it has the same trend as the observed one. This can be explained theoretically using the fact that in the beginning, the number of low-energy electrons is smaller and it increases with an increase in column density. With the increase of low-energy electrons at higher column density, the curve becomes flatter. The same results are obtained over a range of electron and photon energies. However, the calculations are found to be sensitive to the choice of density models. A beam of high-energy electrons injected towards the photosphere will be absorbed in a fraction of seconds. However, we find that rise times are often of the order of afew seconds. There can be two possibilities. First the electrons

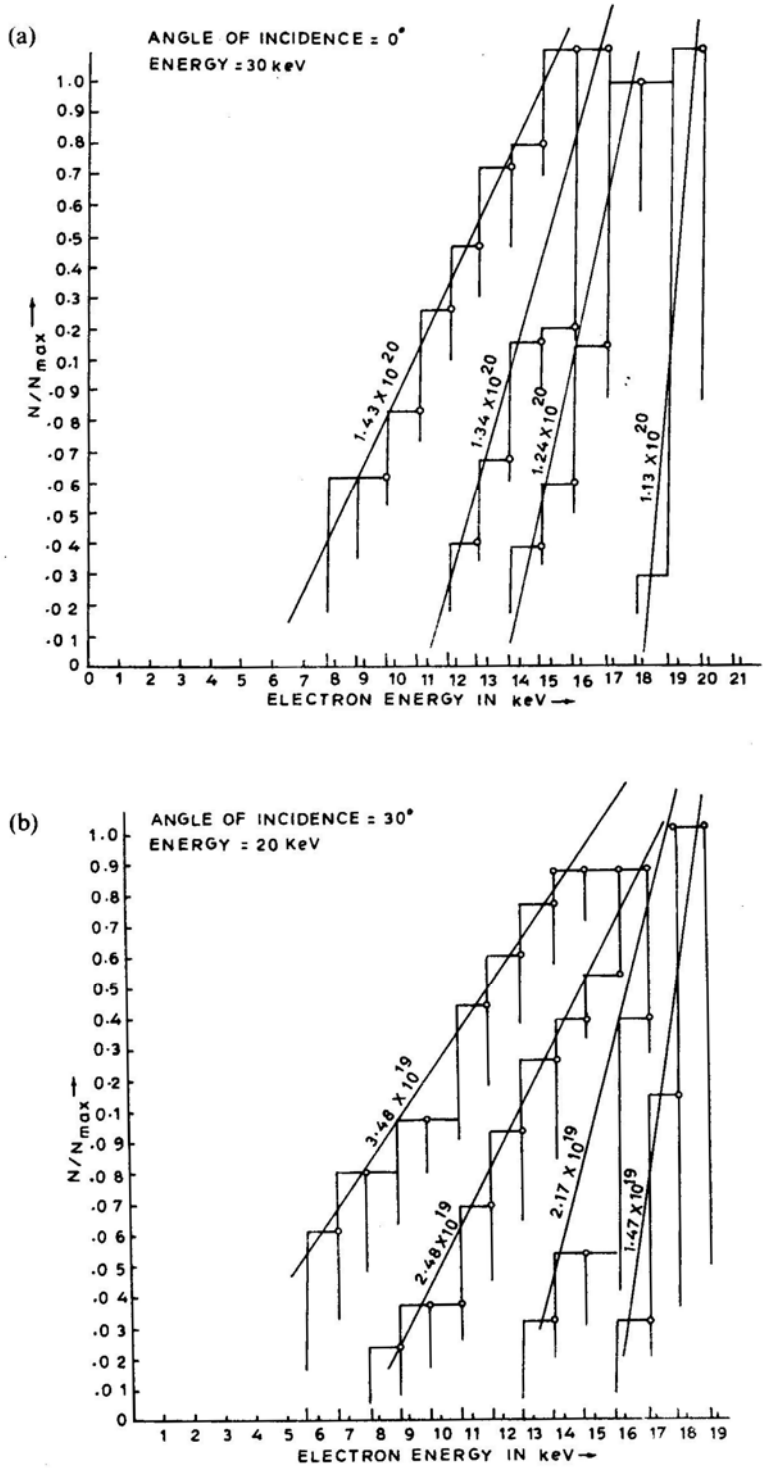

Figure 3. Continued.

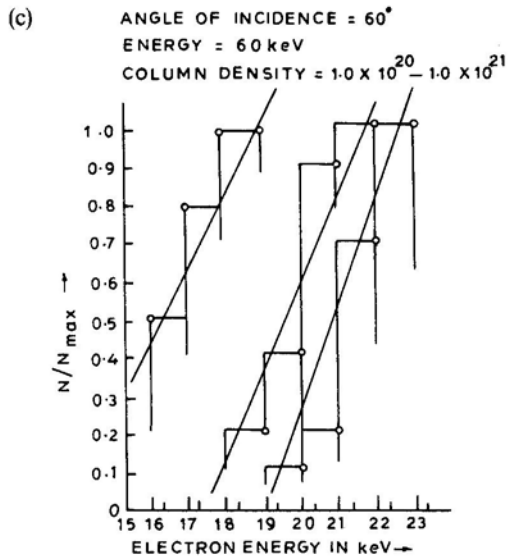

Figure 3. Variation of electron energy distributions and slopes for initial electron energy 20,30, 60 keV incident at 0°, 30° and 60° incidence angles.

coming at higher incidence angles will remain trapped and will keep moving between two conjugate points. Second possibility is that there is continuous injection of the electron beams. The second possibility seems to be more reasonable. Our calculations of hard X-ray spectra and EUV rise times carried out so far favour nonthermal and thick target.

Acknowledgements

We are thankful to Dr. O. N. Kaul, Principal, Regional Engineering College, Srinagar for his keen interest in the work. This work is supported by ISRO Grant No. 10/2/134.

References

Castelli, J. P., Richards, D. W. 1971, *J. Geophys. Res.,* **76,** 8409.
Donnelly, R. F. 1970, ESSA Techn. Rep. ERL 169-SDL 14.
Donnelly, R. F., Wood, A. T., Jr., Noyes, R. W. 1973, *Solar Phys.,* **29,** 107.
Haug, E. 1979, *Solar Phys.,* **61,** 129.
Haug, E., Elwert, G., Rausaria, R. R. 1985, *Astr. Astrophys.,* **146,** 159.
Kane, S. R. 1974, *Space Sci. Lab. Series,* **14,** issue 76.
Kane, S. R., Donnelly, R. F. 1971, *Astrophys. J.,* **164,** 151.
Koul, P. K., Moza, K. L., Khosa, P. N., Rausaria, R. R. 1985, *Astrophys.* J., **292,** 725.
Landini, M., Monsignori Fossi, B. C., Pallavicini, R. 1973, *Solar Phys.,* **29,** 93.
Meekins, J. F., Doschek, G. A., Friedman, H., Chub, T. A., Kreplin, R. W. 1970, *Solar Phys.,* **13,** 198.
Neupert, W. M. 1971, *Solar Phys.,* **18,** 474.
Wood, A. T., Noyes, R. W. 1972, *Solar Phys.,* **24,** 180.